Preprint - 24th European Photovoltaic Solar Energy Conference and Exhibition, Hamburg, Germany, 21-25 Sept. 2009

MODEL-BASED OPTICAL AND ELECTRICAL CHARACTERIZATION OF DYE-SENSITIZED SOLAR CELLS

S. Wenger,[1] M. Schmid,[2] G. Rothenberger,[1] M. Grätzel,[1] J. O. Schumacher[2]
[1]Laboratory of Photonics and Interfaces, Ecole Polytechnique Fédérale de Lausanne (EPFL), EPFL-SB-ISIC-LPI, Station 6, 1015 Lausanne, Switzerland, phone +41 21 693 5178, fax +41 21 693 61 00, e-mail: sophie.wenger@epfl.ch
[2]Institute of Computational Physics (ICP), Zurich University of Applied Sciences (ZHAW), Wildbachstrasse 21, Postfach 805, 8401 Winterthur, Switzerland, phone +41 58 934 6989, fax +41 58 934 7797

ABSTRACT: We present an experimentally validated coupled optical and electrical model for the dye-sensitized solar cell. The light absorption and subsequent charge generation in the photoactive layer is calculated accurately using coherent and incoherent optics. The charge generation function is then used as a source term in the electron continuity equation of the electrical model. The optical model allows to precisely analyze the reflection and absorbance losses in the individual layers. By comparing the calculated and measured quantum efficiency of a test device, one can assess the electron recombination losses at short-circuit conditions. We conclude with an integrated power loss analysis to quantify the contribution of the respective optical and electric loss mechanisms.
Keywords: Dye-Sensitized, Modeling, Optical Losses

1 INTRODUCTION

Dye-sensitized solar cells (DSCs) can convert solar radiation into electricity efficiently and cost-effectively by means of a light-harvesting sensitizer anchored to a high surface area mesoporous semiconductor film [1]. Record efficiencies of over 11% have been achieved with ruthenium-complex sensitizers on laboratory-scale devices [2–4], but progress in efficiency enhancement has been stagnating in the past years. Materials screening and device optimization is often addressed with an empirical approach, which could be greatly accelerated with an accurate simulation of the optical and electric processes in the device.

In this paper we present a comprehensive and experimentally validated model of the DSC, which simulates the light in-coupling into the complete device, the charge generation profile in the photoactive layer, and subsequent transport of charges in the semiconductor film and recombination at its interface. The optical model accounts for multiple reflections and absorbance in the layers of the device using coherent and incoherent optics. In this way, the light intensity, the absorbance, and the charge generation profile in the photoactive layer, are computed accurately. The charge generation function then serves as a source term in the continuity equation for free charge carriers, thus coupling the optical with the electrical model. The model is validated by comparison of simulation results to experimental data. With the aid of the model, we can then analyze the optical losses in the individual device layers and estimate electronic losses due to charge recombination.

The device structure of a DSC is schematically shown in Figure 1. The DSC uses a photoactive sensitizer ("dye") attached to a thin mesoporous TiO_2 film ($< 12\ \mu$m) to harvest the sunlight. The photoexcited dye injects an electron into the TiO_2 conduction band and is rapidly regenerated by a mediator redox couple in the electrolyte, which permeates the pores. The injected electron diffuses through the TiO_2 network to a transparent conducting electrode (fluorine-doped tin oxide, FTO) and migrates through an external electric circuit to the counter electrode, where it regenerates the oxidized mediator.

The issue of the optics of the DSC has been addressed in various studies, but mostly using simplified models lacking experimental validation, and only on parts of the device. Usami studied the light confinement by backscattering from a layer of large TiO_2 particles and total reflection at the front layer by Monte Carlo simulations [5]. Ferber and Luther investigated the enhancement in absorption in mixed TiO_2 films with large and small particles using Mie theory and a numerical solution of the radiative transport equation [6]. By least-squares fitting of a 4-flux model to measured transmittance and reflectance spectra, Rothenberger *et. al.* quantified the absorption and scattering of light in transparent and scattering TiO_2 films [7]. Tachibana *et. al.* simulated the optics of the unsensitized photoanode (glass substrate, conducting electrode, porous TiO_2 film) with the Rouard method using experimentally determined optical constants for the individual layers [8].

Charge generation, transport, and recombination in DSCs is generally described by a continuity equation, in which transport is assumed to be purely diffusive, i.e. driven by concentration gradients only. An analytical solution of the continuity equation for electrons was first given by Södergren *et. al.* [9], and followed by comprehensive models for all species in the complete device [10, 11]. However, time-dependent characterization techniques have later shown that charge transport through the TiO_2 film is impaired by multiple trapping/detrapping events [12]. The present state of electrical modeling is described in extensive reviews by Peter [13] and Bisquert [14].

In this study, the accurate computation of reflectance and absorbance losses in each layer of a complete DSC

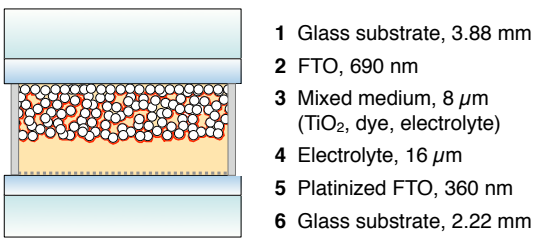

Figure 1: Device structure of the dye-sensitized solar cell depicting the six layers used to model the optics in the device.

allows us to insert a precise charge generation function into the electrical model. We can thus avoid an estimate based on the Lambert-Beer law, as frequently used in other work.

2 EXPERIMENTAL PART AND THEORY

2.1 Device preparation

The device structure of the DSC is shown in Figure 1. Complete test devices were fabricated following standard procedures [15]. The FTO-coated top glass electrode (Nippon Sheet Glass, 10 Ω/□), was first immersed in an aqueous $TiCl_4$ solution to produce a thin TiO_2 charge blocking layer. An ~ 8 μm thick mesoporous layer of 20 nm sized TiO_2 particles was then screen-printed on the treated FTO electrode. The cell geometry was 0.28 cm^2 for test devices and 2×2 cm^2 for optical characterization. The TiO_2 film was sensitized with the ruthenium dye Z907 [16] by overnight immersion in a 0.3 mM solution in a mixture of acetonitrile and *tert*-butanol (volume ratio 1:1). The cell was sealed with a platinized FTO counter electrode (Pilkington, TEC 15, 15 Ω/□) using a 25 μm thick polymer spacer (Surlyn, DuPont). The void was then filled with an iodide/tri-iodide based electrolyte through a hole in the back electrode. The electrolyte consisted of 1.0 M 1,3-dimethylimidazolium iodide, 0.10 M guanidinium thiocyanate, 0.03 M iodine, and 0.5 M *tert*-butylpyridine in a mixture of acetonitrile and valeronitrile (volume ratio 85:15).

2.2 Optical characterization of layers

The optical model requires that the thickness and the complex index of refraction of each layer in the DSC be known.

The film thickness of the FTO films was estimated from cross-sectional scanning electron micrographs. The TiO_2 film thickness was measured with an Alpha-step profilmeter. The optical constants of the FTO glass substrates were determined from etched samples, where the FTO layer was removed with HCl and Zn powder, by fitting the Fresnel equations to measured transmittance and reflectance spectra. Transmittance and reflectance spectra were measured with a spectrophotometer equipped with an integrating sphere. The optical constants of the FTO films were determined using a spectroscopic ellipsometer. The top FTO film (layer **2**) has a strongly textured surface, which impairs the measurement due to depolarization of the incident light beam. Measurements were thus performed on mechanically polished samples to increase accuracy, as proposed by Paulson and Hegedus [17]. Polishing was not necessary for the bottom FTO film (layer **5**).

The layer **3**, consisting of the dye-sensitized mesoporous anatase TiO_2 and the electrolyte permeating the pores, was treated as a mixed medium with an effective complex index of refraction ($\tilde{n}_e = n_e + ik_e$) using the Bruggeman effective medium approximation [18]. The mixed medium was described as a mixture of medium **3a** ($\tilde{n}_a$), the electrolyte, and medium **3b** ($\tilde{n}_b$), a fictitious TiO_2/dye phase. The porosity of the mesoporous film is known from BET measurements to be $P = 0.68$. The effective complex index of refraction, $\tilde{n}_e$, then satisfies

$$P\frac{\tilde{n}_a^2 - \tilde{n}_e^2}{\tilde{n}_a^2 + 2\tilde{n}_e^2} + (1-P)\frac{\tilde{n}_b^2 - \tilde{n}_e^2}{\tilde{n}_b^2 + 2\tilde{n}_e^2} = 0. \qquad (1)$$

For medium **3a**, n_a was taken from literature values for acetonitrile [19], and k_a was derived from absorbance measurements of tri-iodide in acetonitrile, which is the only absorbing species in the electrolyte. For medium **3b**, n_b was taken from literature values for anatase [20], and k_b was back calculated from Equation (1). The effective imaginary index k_e was experimentally determined by using a four-flux model analysis on transmittance and reflectance spectra of a simplified stack, where the two FTO electrodes were replaced by microscope glasses, and the electrolyte was replaced by acetonitrile [7]. The remaining unknown parameters, i.e. n_e and k_b, were determined by solving Equation 1.

The thin layer of platinum particles on the back electrode is virtually transparent and its optical effect was thus neglected in this study.

2.3 Photovoltaic Characterization

The external quantum efficiency of test devices was measured using light from a 300 W xenon lamp focused through a Gemini-180 double monochromator. The photon flux of light incident on the devices was measured using a calibrated silicon photodiode with a spectral response modified to approximately match the absorption profile of the Z907 dye. The photocurrent was measured using a Keithley 2400 source meter. The current-voltage curve of devices was measured by illuminating with light from a 450 W xenon lamp matched to AM 1.5G sunlight irradiation with filters in the range of 350–750 nm. Beam intensity was calibrated with a silicon photodiode. The current and voltage were measured and controlled with a Keithley 2400 source meter. Various incident light intensities were varied with wavelength neutral wire mesh attenuators. The photoactive area of 0.158 cm^2 was defined with a metal mask.

2.4 Optical Model

The optical model is based on a ray-tracing algorithm [21]. The model domain represents the device structure shown in Figure 1. The thicknesses of the six layers of the stack and their complex indices of refraction must be given as input. The ray-tracing algorithm calculates the geometric path of a monochromatic light ray through the model domain. The rays sent out from a light source are traced as they propagate through the optical stack. This procedure is repeated for different wavelenghts. The light intensity of an incident ray is reduced successively due to external reflection and light absorption within the layers. The algorithm accounts for multiple reflections within the stack. The two FTO films (layers **2** and **5**) are treated using coherent optics. All the other layers are treated using geometrical optics. The reflection and transmission coefficients at the interfaces are calculated using a transfer matrix approach [22].

The net photon flux $\phi_\lambda(x)$ at any position in the stack (the x-axis is defined as perpendicular to the interfaces) for a given wavelength λ is given by the sum of the forward flux $\phi_\lambda^+(x)$ and the reflected backward flux $\phi_\lambda^-(x)$. One can then calculate the number of absorbed photons per unit of time and volume in the sensitized TiO_2 film using

$$G_\lambda(x) = \alpha(\lambda)\left(\phi_\lambda^+(x) + \phi_\lambda^-(x)\right), \qquad (2)$$

where $\alpha(\lambda)$ is the absorption coefficient of the dye. The fraction of incident photons, per unit of length, absorbed

at position x is given by

$$g(\lambda, x) = \frac{G_\lambda(x)}{\phi_{\lambda,inc}}, \tag{3}$$

where $\phi_{\lambda,inc}$ is the incident photon flux. By integrating $g(\lambda, x)$ over the TiO_2 film thickness interval $[0, d]$, where d is the film thickness, we find the total fraction of absorbed light in the film at wavelength λ (or the maximum achievable external quantum efficiency),

$$f_{abs}(d, \lambda) = \int_0^d g(\lambda, x)\, dx. \tag{4}$$

By integrating $G_\lambda(x)$ over the whole spectral range and multiplying with an injection efficiency η_{inj}, we find the spatially resolved electron injection rate

$$G_e(x) = \eta_{inj}\, G(x), \quad \text{where} \quad G(x) = \int_0^\infty G_\lambda(x)\, d\lambda. \tag{5}$$

We initially assume that $\eta_{inj} = 1$, independent of λ, i.e. every absorbed photon is converted to an injected electron in the TiO_2 conduction band.

$G_e(x)$ then serves as a source term for the electrical model. In addition, we obtain the maximum achievable short circuit current density using

$$j_{max} = e \int_0^d G_e(x)\, dx, \tag{6}$$

where e is the elementary charge.

2.5 Electrical model

The electrical model is based on the continuity equation for the electron number density $n(x)$ in the conduction band of the TiO_2 layer and on a purely diffusive transport equation for the electrical current density j [9]:

$$-\frac{1}{e}\frac{dj}{dx} = G_e(x) - U(x), \tag{7}$$

$$j = eD\,\frac{dn}{dx}, \tag{8}$$

where $G_e(x)$ is the electron injection rate, determined from the optical model, $U(x)$ is the recombination rate, and D is the diffusion coefficient for conduction band electrons. We assume that only electrons from the conduction band can recombine with tri-iodide in the electrolyte and that the recombination rate is linear in $n(x) - \bar{n}$,

$$U(x) = \frac{n(x) - \bar{n}}{\tau}. \tag{9}$$

Here, τ is the lifetime of the conduction band electrons and $\bar{n}$ is the electron number density at equilibrium in the dark.

Combining Equations (7), (8), and (9) leads to an inhomogeneous linear differential equation for $n(x)$,

$$L^2\frac{d^2n}{dx^2} - (n(x) - \bar{n}) + \tau\, G_e(x) = 0, \tag{10}$$

where $L = \sqrt{D\tau}$ is the electron diffusion length. This study is restricted to the analysis of the external quantum efficiency of test devices, which is measured under steady-state conditions. If the quasi-equilbrium approximation is used (one single quasi-Fermi level for conduction band and trapped electrons), then, under steady-state conditions, the continuity equation does not include terms due to trapping/detrapping. The diffusion length is then given by a constant [12]. The boundary conditions to Equation (10) are

$$n(0) = N_c\, f(E_c, E_{F0} + eV) \quad \text{and} \quad \left.\frac{dn}{dx}\right|_{x=d} = 0, \tag{11}$$

where V is the applied voltage, N_c is the total density of conduction band states, f is the Fermi-Dirac distribution, E_c is the conduction band energy, and E_{F0} is the Fermi level in the dark. For the sake of generality, we use a Fermi-Dirac distribution to estimate the electron density at $x = 0$. Setting $V = 0$, we obtain the short-circuit case. The open-circuit voltage is calculated from the condition

$$\left.\frac{dn}{dx}\right|_{x=0} = 0. \tag{12}$$

The homogeneous part of (10) can be solved analytically,

$$n_h(x) = a \exp(-x/L) + b \exp(x/L), \tag{13}$$

where a and b are constants determined by the boundary conditions. A particular solution of Equation (10) can be computed using its Green's function defined by

$$L^2\frac{d^2\mathcal{G}}{dx^2} - \mathcal{G}(x) = \delta(x). \tag{14}$$

The particular solution then is the convolution of the Green's function[1] with the electron injection rate,

$$n_p(x) = -\tau \int_0^d \mathcal{G}(x - y)\, G_e(y)\, dy. \tag{15}$$

From the complete solution

$$n(x) = n_h(x) + n_p(x), \tag{16}$$

the current density at short circuit can be calculated by

$$j_{sc} = e\, D \left.\frac{dn}{dx}\right|_{x=0} \quad \text{for} \quad V = 0. \tag{17}$$

The external quantum efficiency (EQE) is simulated using monochromatic light of wavelength λ_0 and incident photon flux density ϕ_0 to calculate the injected charge generation rate,

$$G_\delta(x) = \eta_{inj}\, \phi_0 \int_0^\infty \delta(\lambda - \lambda_0)\, g(\lambda, x)\, d\lambda \tag{18}$$

$$= \eta_{inj}\, \phi_0\, g(\lambda_0, x). \tag{19}$$

The EQE is then derived from the calculated j_{sc} by inserting $G_\delta(x)$ in Equation (15),

$$EQE(\lambda) = \frac{j_{sc}}{e\,\phi_0}. \tag{20}$$

The parameters of the electrical model are L, τ, N_c, and the difference $E_c - E_{F0}$ between the conduction band edge and the Fermi level in the dark. In this study L is a fitting parameter. The other parameters were taken from the literature [23]. The values are $\tau = 2$ ms, $N_c = 2 \times 10^{20}$ cm^{-3}, and $E_c - E_{F0} = 0.9$ eV.

[1] One can easily show by using Fourier transforms, that the Green's function in (14) is given by

$$\mathcal{G}(x) = -\frac{1}{2L}\left[H(-x)\exp(x/L) + H(x)\exp(-x/L)\right],$$

where $H(x)$ is the unit step function.

3 RESULTS AND DISCUSSION

3.1 Simulation of transmittance and reflectance spectra

Figure 2a shows a comparison of the measured and simulated transmittance and reflectance spectra of a complete device as depicted in Figure 1. The measured and simulated spectra are in good agreement, providing a first experimental validation of the optical model. We attribute the small differences mainly to the inaccurate optical constants of the FTO films and to scattering effects at the FTO/TiO_2 interface, which we do not account for in the present model. Indeed, the simulated and measured spectra of the FTO electrodes only do not match completely.

Figure 2b shows the measured and simulated transmittance and reflectance spectra of a simplified stack with dye-sensitized TiO_2 and electrolyte sandwiched between two 1 mm thick microscope glasses. In this case, the agreement between the measurement and the simulation is excellent. The optics in the mixed mesoporous medium can thus be well described by a Bruggemann effective medium approach and the ray-tracing algorithm as described in Section 2.4.

3.2 Optical loss analysis

The optical simulation allows to separate the different optical loss channels. Figure 3 shows the calculated fraction of absorbed light by the dye f_{abs}, the total reflection losses, and the absorbance losses in the FTO and electrolyte layers. At 520 nm, which corresponds to the maximum of the dye absorption coefficient, f_{abs} exhibits a maximum of 90%, 7% of the incident light is reflected, and less than 1% is absorbed in the front FTO layer. For the specific device considered here, the main optical losses between 400 nm and 800 nm are caused by reflection (no anti-reflective coating) and to a smaller extent by the absorption in the FTO of the top glass electrode. The absorption in the electrolyte is negligible, apart from a very small contribution between 400 nm and 500 nm due to tri-iodide. However, even between 500 nm and 600 nm, at the maximum of the dye absorption, there is still a small amout of light transmitted. In state-of-the-art devices, this loss is reduced by using thicker films (up to 12 μm) and adding a strongly backscattering layer of 400 nm sized particles to the film [15].

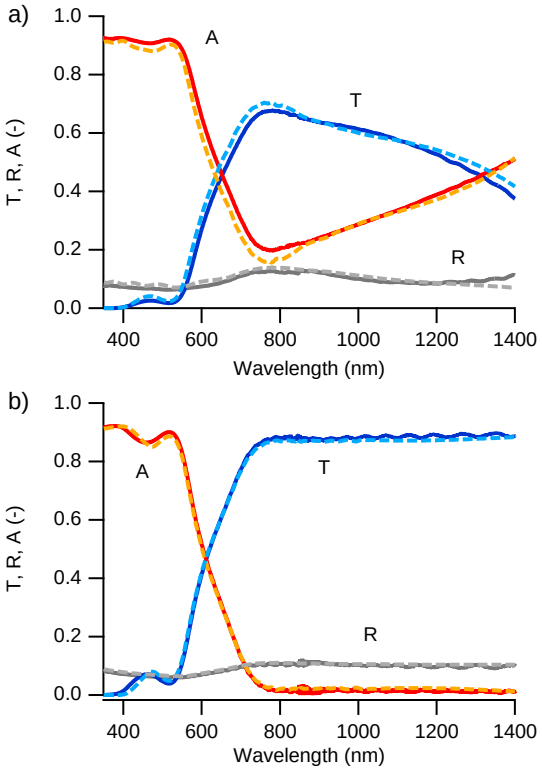

Figure 2: Total transmittance (T), reflectance (R), and absorbance ($A = 1 - T - R$) spectra of a *complete device* (a) and a *simplified stack* (b). Measurements are represented by bold lines and simulations by dashed lines.

3.3 Simulation of the external quantum efficiency

In Figure 4 the maximum achievable external quantum efficiency (EQE) f_{abs} is compared with the measured EQE and the simulated EQE from the electrical model. The difference between the calculated fraction of absorbed photons and the measured fraction of extracted electrons is strikingly large. At 520 nm, 90% of the incident photons are absorbed by the dye, but only 72% of the incident photons are extracted as electrons. 18% of the incident photons are thus lost due to one (or a combination) of the following reasons: (a) The injection efficiency may be smaller than unity. (b) The dye may form aggregates, which absorb light but are not attached to the TiO_2 surface and do not inject into the TiO_2. (c) Injected electrons in the TiO_2 conduction band may recombine with oxidized dye species. (d) Injected electrons may recombine with tri-iodide at the TiO_2/electrolyte interface during transport through the film. Laser transient absorbance studies on TiO_2 films sensitized with Z907 dye have shown injection efficiencies $n_{inj} \approx 0.9 - 1.0$ (depending on the presence of Li^+ cations, which can lower the TiO_2 conduction band upon adsorption on the surface and facilitate injection) and negligible recombination between injected electrons and dye cations [24]. Dye desorption studies have shown that the TiO_2 surface coverage is $\leq 100\%$, making the presence of aggregates improbable. The comparison of f_{abs} and the measured EQE thus indicates, that even under short-circuit conditions a large fraction of electrons recombines with tri-iodide.

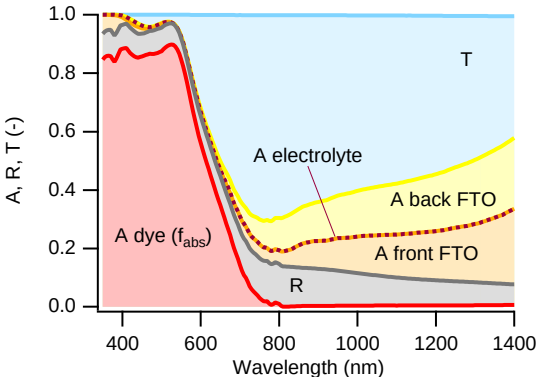

Figure 3: Calculated fractions of absorbed, reflected, and transmitted light in a test device: Absorbed light by dye (red), front FTO layer (orange), back FTO layer (yellow), and electrolyte (dotted brown line), total reflection loss (grey), and total transmitted light (blue).

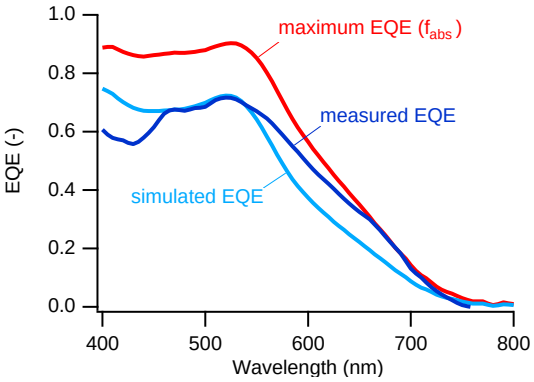

Figure 4: Comparison of the maximum achievable EQE f_{abs} obtained with the optical model, the measured EQE of a test device, and the calculated EQE obtained from the coupled optical and electric model using a electron diffusion length of $L = 6.3\ \mu$m and an injection efficiency of unity.

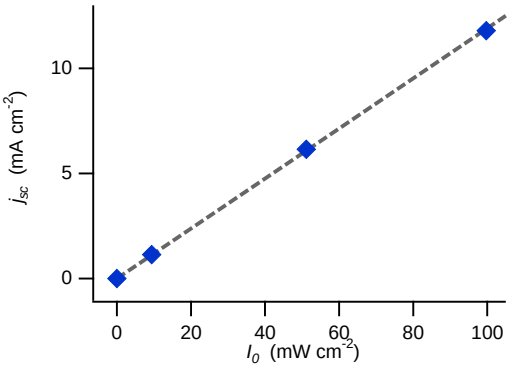

Figure 5: Measured (blue diamonds) and simulated (dashed grey line) short circuit current density j_{sc} as a function of incident light intensity I_0 for an electron diffusion length $L = 6.3\ \mu$m.

The recombination rate can be quantified by adjusting the diffusion length parameter in Equation (10) such that the peak value at 520 nm of the calculated EQE matches the measured EQE. Assuming $n_{inj} = 1$, we find a relatively short diffusion length of $L = 6.3\ \mu$m. For $n_{inj} = 0.9$, we get $L = 9.0\ \mu m$. The values for the diffusion length parameter determined in this way must be regarded as an average over the whole TiO_2 film thickness, since our model uses a constant and not a position dependent L. However, the charge density in the film varies strongly under short-circuit conditions [13]. The mismatch between the measured and calculated EQE in the range $\lambda = 550 - 750$ nm is due to small uncertainties in the determination of the optical constants of the FTO films and the scattering at the FTO/TiO_2 interface (see Section 3.1 and Figure 2 a).

The accurate determination of f_{abs}, which is validated by the good fits in Figure 2, allows to further separate the optical and electrical losses. At 520 nm, 10% of the incident light is lost due to reflection and absorption by the front FTO electrode as described in Section 3.2. For $n_{inj} = 1$, additional 18% is lost due to recombination of injected electrons with tri-iodide. For $n_{inj} = 0.9$, 9% is lost via radiative decay of the excited sensitizer state, and the remaining 9% is lost due to recombination. In either case, the recombination losses under short-circuit conditions are not negligable.

3.4 Simulated short-circuit current

In Figure 5 we compare the calculated and measured short-current density j_{sc} at different illumination intensities. For the calculation, the spectrum of a xenon lamp filtered to match AM 1.5G conditions was used as incident light, and the diffusion length was fixed to $L = 6.3\ \mu$m. The excellent agreement between the calculated and measured values further validates the coupled optical and electric model. j_{sc} increases linearly with light intensity as expected. In our model, the parameter L can be regarded as constant and independent of illumination intensity at short-circuit conditions.

3.5 Integrated power loss analysis

The device considered here exhibited a conversion efficiency of 6.6%, a j_{sc} of 11.8 mA cm^{-2}, an open-circuit voltage of 755 mV, and a fill factor of 0.74 under simulated AM 1.5G illumination (100 mW cm^{-2}). Hence, the device produced 6.6 mW cm^{-2} when operated at its maximum power point. In the following, we attempt to explain by which processes the 93.4% of incident energy are lost.

The incident power of AM 1.5G illumination, integrated over the whole spectral range ($\lambda = 280 - 4000$ nm), equals 100 mW cm^{-2}. From integration of the product of f_{abs} and the AM 1.5G spectrum, we find an absorbed power of 32.5 mW cm^{-2} and a maximum achievable j_{sc} of 13.6 mA cm^{-2}. Thus 67.5% of incident power are not absorbed by the dye.

From integration of the product of the measured EQE and the AM 1.5G spectrum we find an extracted power density of 25.8 mW cm^{-2} (corresponding to a j_{sc} of 10.8 mA cm^{-2}). Further 6.7% of the incident power are thus lost via relaxation of excited sensitizers states and recombination of injected electrons with tri-iodide.

The remaining 19.2% of power density loss constitute a loss of electron potential energy via thermalization from at most 3.1 eV (400 nm) to at most 0.76 eV (in open-circuit conditions).

4 CONCLUSIONS

We have demonstrated the utility of an accurate, experimentally validated, coupled optical and electrical model of a complete DSC to separate and quantify the respective optical and electrical losses. A precise optical loss analysis has shown that the absorbance in the dye-sensitized TiO_2 film is predominantly attenuated by reflection losses. Absorbance losses in the FTO layer or by tri-iodide in the electrolyte are marginal. Optical losses are thus most effectively reduced by using anti-reflective coatings on the front electrode, e.g. fluorinated polymer films [15].

From comparison of measured and calculated external quantum efficiency we found a short electron diffusion length in the range of the film thickness. This indicates a high recombination rate of electrons with tri-iodide even under short-circuit conditions. The fraction of photons lost due to relaxation of the excited sensitizers, i.e. the injection rate for the specific system considered here, remains to be assessed precisely but is expected to be close to unity. Electrical losses are thus best reduced by inhibiting the re-

combination mechanism with tri-iodide, e.g. with suitable co-adsorbants on the TiO_2 surface.

Finally, an integrated power loss analysis has shown, that the largest fractions of power are lost due to low light absorption and electron potential energy loss via thermalization. Further experimental work is thus necessary to enhance the spectral response of sensitizers to the near-infrared region and to increase the electron potential energy, e.g. with novel redox systems with more positive redox potential.

We believe, this coupled model will be a valuable complementary tool to identify and minimize optical and electrical losses, to screen novel materials and device architectures rapidly and accurately, and to accelerate the development of this promising technology.

ACKNOWLEDGMENTS

We thank Pascal Comte for TiO_2 film preparation, Shaik M. Zakeeruddin for electrolyte and dye solution, Frédéric Sauvage for taking the scanning electron micrographs, Didier Bouvet for mechanical polishing of the front FTO electrode, and Philippe Langlet for assistance with ellipsometry measurements (all EPFL). Financial support by the GERBERT RÜF STIFTUNG (project No. GRS-064/07) and the Swiss National Science Foundation (project No. NF 20020-125163/1) is gratefully acknowleged.

REFERENCES

[1] M. Grätzel, Nature 414 (2001) 338.
[2] M. K. Nazeeruddin, F. De Angelis, S. Fantacci, A. Selloni, G. Viscardi, P. Liska, S. Ito, B. Takeru, M. Grätzel, Journal of the American Chemical Society (2005) 16835.
[3] Y. Chiba, A. Islam, Y. Watanabe, R. Komiya, N. Koide, L. Han, Japanese Journal of Applied Physics, Part 2: Letters 45 (2006).
[4] F. Gao, Y. Wang, D. Shi, J. Zhang, M. K. Wang, X. Y. Jing, R. Humphry-Baker, P. Wang, S. M. Zakeeruddin, M. Grätzel, Journal of the American Chemical Society 130 (2008) 10720.
[5] A. Usami, Chemical Physics Letters 277 (1997) 105.
[6] J. Ferber, J. Luther, Solar Energy Materials and Solar Cells 54 (1998) 265.
[7] G. Rothenberger, P. Comte, M. Grätzel, Solar Energy Materials and Solar Cells 58 (1999) 321.
[8] Y. Tachibana, H. Y. Akiyama, S. Kuwabata, Solar Energy Materials and Solar Cells 91 (2007) 201.
[9] S. Soedergren, A. Hagfeldt, J. Olsson, S.-E. Lindquist, The Journal of Physical Chemistry 98 (1994) 5552.
[10] J. Ferber, R. Stangl, J. Luther, Solar Energy Materials and Solar Cells 53 (1998) 29.
[11] N. Papageorgiou, M. Grätzel, P. P. Infelta, Solar Energy Materials and Solar Cells 44 (1996) 405.
[12] J. Bisquert, V. S. Vikhrenko, The Journal of Physical Chemistry B 108 (2004) 2313.
[13] L. M. Peter, The Journal of Physical Chemistry C 111 (2007) 6601.
[14] J. Bisquert, Physical Chemistry Chemical Physics 10 (2008) 49.
[15] S. Ito, T. N. Murakami, P. Comte, P. Liska, C. Grätzel, M. K. Nazeeruddin, M. Grätzel, Thin Solid Films 516 (2008) 4613.
[16] P. Wang, S. M. Zakeeruddin, J. E. Moser, M. K. Nazeeruddin, T. Sekiguchi, M. Grätzel, Nature Materials 2 (2003) 402.
[17] P. D. Paulson, S. S. Hegedus, Journal of Applied Physics 96 (2004) 5469.
[18] D. A. G. Bruggeman, Annalen der Physik 24 (1935) 636.
[19] I. Z. Kozma, P. Krok, E. Riedle, Journal of the Optical Society of America B 22 (2005) 1479.
[20] H. Tang, H. Berger, P. E. Schmid, F. Lévy, Solid State Communications 92 (1994) 267.
[21] J. O. Schumacher, Numerical simulation of silicon solar cells with novel device structures, PhD thesis, University of Konstanz (2000).
[22] M. Born, E. Wolf, Principles of optics: electromagnetic theory of propagation, interference and diffraction of light, Cambridge University Press, Cambridge, UK, 7th edition (1999).
[23] U. Würfel, M. Peters, A. Hinsch, The Journal of Physical Chemistry C 112 (2008) 1711.
[24] P. Wang, S. M. Zakeeruddin, J.-E. Moser, M. Grätzel, The Journal of Physical Chemistry B 107 (2003) 13280.